crystals

Article

Mechanical Performance and Microscopic Mechanism of Coastal Cemented Soil Modified by Iron Tailings and Nano Silica

Xinjiang Song [1], Haibo Xu [1], Deqin Zhou [2], Kai Yao [3], Feifei Tao [4], Ping Jiang [2] and Wei Wang [2,]*

[1] Department of Geotechnical Engineering, Anhui and Huaihe River Water Resources Research Institute, Bengbu 233000, China; sxj06@163.com (X.S.); hbxu2006@163.com (H.X.)
[2] School of Civil Engineering, Shaoxing University, Shaoxing 312000, China; zhoudeqinusx@163.com (D.Z.); jiangping@usx.edu.cn (P.J.)
[3] School of Qilu Transportation, Shandong University, Jinan 250002, China; yaokai@sdu.edu.cn
[4] School of Chemistry and Chemical Engineering, Shaoxing University, Shaoxing 312000, China; feifeitao@usx.edu.cn
* Correspondence: wellswang@usx.edu.cn

Abstract: In order to explore the effect of composite materials on the mechanical properties of coastal cement soil, cement soil samples with different iron tailings and nano silica contents were prepared, and unconfined compression and scanning electron microscope tests were carried out. The results show that: (1) The compressive strength of cement soil containing a small amount of iron tailings is improved, and the optimum content of iron tailings is 20%. (2) Nano silica can significantly improve the mechanical properties of iron tailings and cement soil (TCS). When the content of nano silica is 0.5%, 1.5%, and 2.5%, the unconfined compressive strength of nano silica- and iron tailings-modified cement soil (STCS) is 24%, 137%, and 323% higher than TCS, respectively. (3) Nano silica can promote the hydration reaction of cement and promote the cement hydration products to adhere to clay particles to form a relatively stable structure. At the same time, nano silica can fill the pores in TCS and improve the compactness of STCS.

Keywords: coastal cemented soil; nano silica; iron tailings; mechanical properties; microscopic mechanism

Citation: Song, X.; Xu, H.; Zhou, D.; Yao, K.; Tao, F.; Jiang, P.; Wang, W. Mechanical Performance and Microscopic Mechanism of Coastal Cemented Soil Modified by Iron Tailings and Nano Silica. *Crystals* **2021**, *11*, 1331. https://doi.org/10.3390/cryst11111331

Academic Editors: Shujun Zhang, Cesare Signorini, Antonella Sola, Sumit Chakraborty and Valentina Volpini

Received: 6 October 2021
Accepted: 28 October 2021
Published: 31 October 2021

1. Introduction

Cemented soil has the advantages of high compressive strength [1], low permeability, and low price. It has been widely used in projects such as soft soil foundation reinforcement, high-grade highway cushions, and seepage prevention in small reservoirs, among other projects, and has achieved good engineering benefits [2]. However, in practical engineering, it was found that coastal cemented soil (CS) cannot meet the mechanical requirements of some large-scale and special coastal engineering projects. For example, Liu et al. studied the heterogeneity in strength and Young's modulus of cement-admixed clay slabs using random finite-element analyses, considering three sources of variation: namely, a deterministic radial trend in strength and Young's modulus; a stochastic fluctuation component due to non-uniform mixing; and positioning errors arising from off-verticality of the mixing shafts [3]. Li et al. studied the influence of the number of freeze–thaw cycles and curing ages on the mechanical properties of ordinary cemented clay and polypropylene fiber-cemented clay [4]. Liu et al. examined the interaction between the spatial variations in binder concentration and in situ water content, in cement-mixed soil, using field and model data as well as statistical analysis and random field simulation [5]. The results of these studies suggest that it is necessary to add additives to modify the coastal cemented soil. On the other hand, as an industrial by-product, the annual output of iron tailings in China is huge. The accumulation of iron tailings not only takes up farmland and pollutes the environment, but also tends to cause dangerous accidents such as collapses with the increasing of the accumulation height. The use of iron tailings to make composite cemented soil, and at the same time adulterating new admixtures to meet the requirements of engineering mechanics, can not only reduce environmental pollution [6], but also save building materials so as to achieve the dual benefits of economic efficiency and environmental protection, which is a very effective way to achieve sustainable development [7].

Extensive research studies on TCS have been conducted by scholars at home and abroad. Lucas et al. compared the effects of cement, lime, and slag composite iron tailings as roadbed fillers, and found that cement was the most effective stabilizer of iron tailings through unconfined compressive tests [8]. Bastos et al. found through CBR tests that cement composite iron tailings had satisfactory physical and mechanical properties, and thus, were suitable for road bases under most traffic loads with good durability [9]. Through compressive and flexural tests, Hou Rui et al. found through compressive and flexural tests that the compressive and flexural strengths of TCS increased gradually with age, but increased slowly in the later stage. When the iron tailing content was less than 25%, the mechanical properties of TCS were slightly increased compared with that of CS [10].

In recent years, many scholars have tried to develop new engineering materials by compounding various curing agents with iron tailings. Generally, cement can be used to improve the mechanical properties of iron tailings. Tanko et al. studied the performance of cement concrete mixed with fine aggregate of iron tailings [11]. Bao et al. studied the toughening properties of sand cement-based composites of high-performance environmentally friendly tailings [12]. Simonsen et al. studied mine tailings' potential as supplementary cementitious materials based on their chemical, mineralogical and physical characteristics [13]. Long et al. carried out research on the mechanical properties and durability of coal gangue-reinforced cement–soil mixture for foundation treatments [14]. On this basis, lime, slag, fiber, etc. can be added to further improve the mechanical properties of cement-modified iron tailings. Consoli et al. studied fiber-reinforced sand-coal fly ash-lime-NaCl blends under severe environmental conditions [15]. Feng et al. studied lime-and cement-treated sandy lean clay for highway subgrade in China [16]. Tebogo et al. studied mechanical chemically treated and lime-stabilized gold mine tailings using unconfined compressive strength [17]. Kumar et al. studied the use of iron ore tailings, slag sand, ground granular blast furnace slag, and fly ash to produce geopolymer bricks [18]. Falayi et al. conducted a comparative study on the mechanical properties of geological polymers of gold mine tailings modified by fly ash and alkaline oxygen slag [19]. Festugato et al. studied the cyclic shear behavior of fiber-reinforced mine tailings [20]. Chen et al. studied the compressive behavior and microstructural properties of tailings polypropylene fiber-reinforced cemented paste backfill [21]. Cristelo et al. studied the effect of fiber on the cracking behavior of cement-stabilized sandy clay under indirect tensile stress [22]. Lirer et al. studied the strength of fiber-reinforced soils [23]. Among them, cement is the traditional building material with the best modification effect, but it still cannot fully meet the engineering needs. Therefore, it is urgent to find a composite admixture to improve the engineering characteristics of TCS. Nanomaterials have the characteristics of large specific surface area, small particles, and high activity. Therefore, they have been introduced into the engineering exploration of TCS. For example, Ghasabkolaei et al. summarized the geotechnical properties of soil modified by nanomaterials [24]. Wang et al. studied characterization of nano magnesia–cement-reinforced seashore soft soil by direct-shear test [25]. Yao et al. studied effect of nano-MgO on the mechanical performance of cement-stabilized silty clay [26]. It has been found through various studies that nanomaterials can fully exert their own activity in cement-based materials, promote the process of cement hydration reaction, and fully fill the internal pores of cement-based materials at the microscopic scale, thus achieving the purpose of improving the engineering properties of cement-based materials. For example, Zheng et al. studied strength and hydration products of cemented paste backfill from sulfide-rich tailings using reactive MgO-activated slag as a binder [27]. Liu et al. studied the effect of graphite tailings as a substitute for sand on the mechanical properties of concrete [28]. Sarkkinen et al. studied the efficiency of MgO-activated GGBFS and OPC in the stabilization of highly sulfidic mine tailings [29]. Through an indoor unconfined compressive test combined with a microscopic test, Li et al. found that the use of nano clay instead of cement in iron tailings can effectively improve its compressive strength. The addition of nano clay makes the microstructure surface of TCS change from flake to block; the granular structure becomes tightly cemented, and the whole structure tends to be stable [30]. Nano clay can improve the mechanical properties of TCS and can guide the resource application of iron tailings to a certain extent. It is feasible to apply nanomaterials to engineering practice. Due to its unique physical properties, nano silica has also recently been widely used in geotechnical engineering, for example, in modified calcareous sand in the South China Sea [31] and in stabilized coastal silty clay [32].

Therefore, the research on STCS has important theoretical significance and engineering application value, and microstructure has a certain influence on the mechanical properties of materials [33]. In this paper, the optimal iron tailing content was explored through unconfined compressive tests, the modification effect of nano silica on TCS was studied, and the strength growth mechanism of STCS was analyzed in combination with microscopic tests.

2. Test Overview

2.1. Test Materials

The soil used in this experiment was collected from the coastal soft subgrade soil excavated in a certain expressway section in Shaoxing city, Zhejiang. The physical and mechanical indexes are shown in Table 1, and the microscopic characteristics are shown in Figure 1. The main chemical elements of the soil are Si, O, Mg, and Al. The natural state of the soil is a soft plastic state, with high porosity and organic matter content. The iron tailings were taken from Lizhu iron tailings pond in Zhejiang Province. The physical and mechanical indexes are shown in Table 2, and the microscopic characteristics are shown in Figure 2. The main chemical elements of iron tailings are Si, O, Mg, and C, and their particles are small and single. PO 32.5 Conch brand Portland cement, produced in Shangyu, Shaoxing, was used in this test. The physical and mechanical indexes are shown in Table 3, and the microscopic characteristics are shown in Figure 3. The cement's performance meets requirements and it can be used to modify soft soil. Ordinary industrial nano silica was used in this test. The physical and mechanical indexes are shown in Table 4, and the microscopic characteristics are shown in Figure 4. The nano silica used in the test is pure, its microstructure is dense, and it has a large specific surface area.

Table 1. Physical and mechanical indexes of coastal soft soil.

Natural Moisture Content %	Volume Weight g/cm^3	Void Ratio	Saturation Degree %	Plastic Limit ω_P%	Liquid Limit ω_L%	Plasticity Index I_P	Liquidity Index I_l	Organic Content (%)
58	1.63	1.74	98	25	47	22	1.34	6.5

Table 2. Physical and mechanical indexes of iron tailings.

Index	Loss on Ignition (%)	Specific Gravity	Specific Area (m^2/kg)	Liquid Limit (%)	Plastic Limit (%)
Value	7.01	3.06	379	23	17

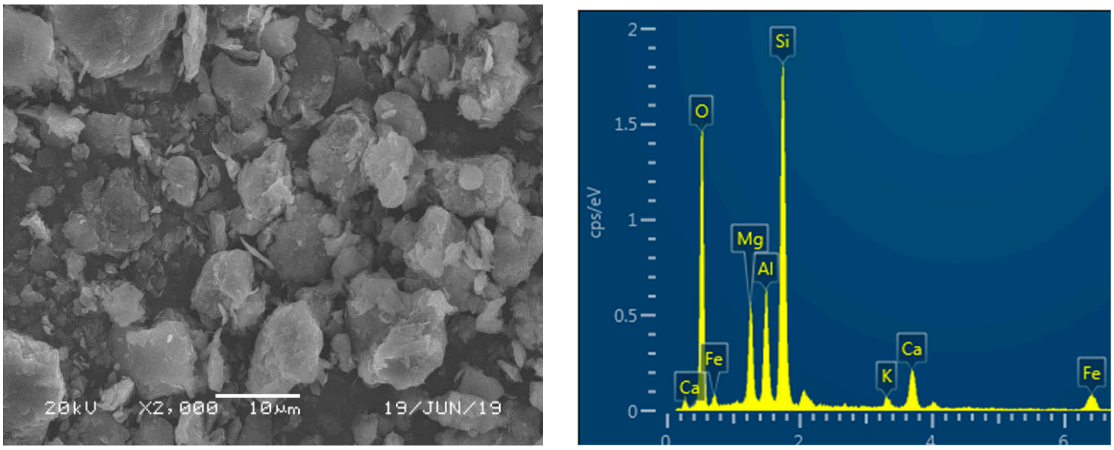

(**a**) (**b**)

Figure 1. (**a**) SEM, (**b**) EDS. Microscopic characteristics of coastal soft soil.

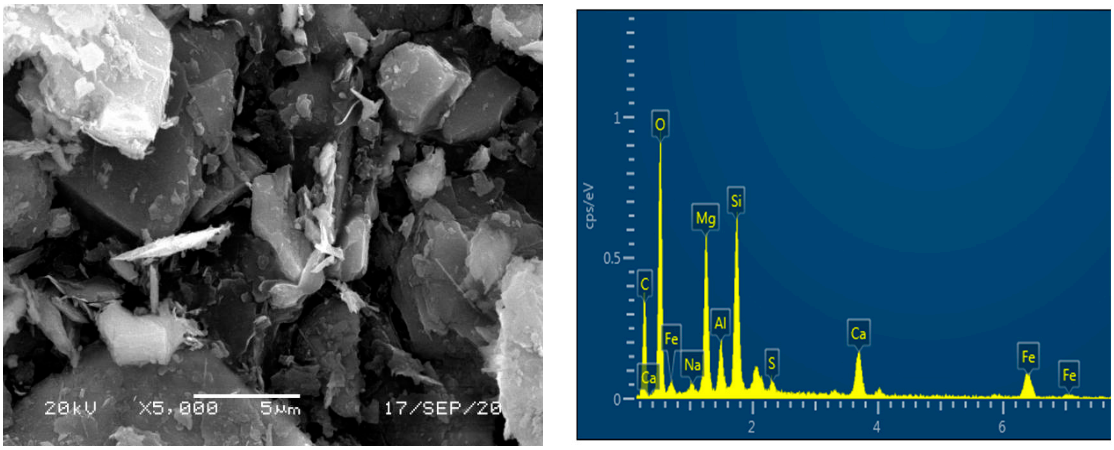

(**a**) (**b**)

Figure 2. (**a**) SEM, (**b**) EDS. Microscopic characteristics of iron tailings.

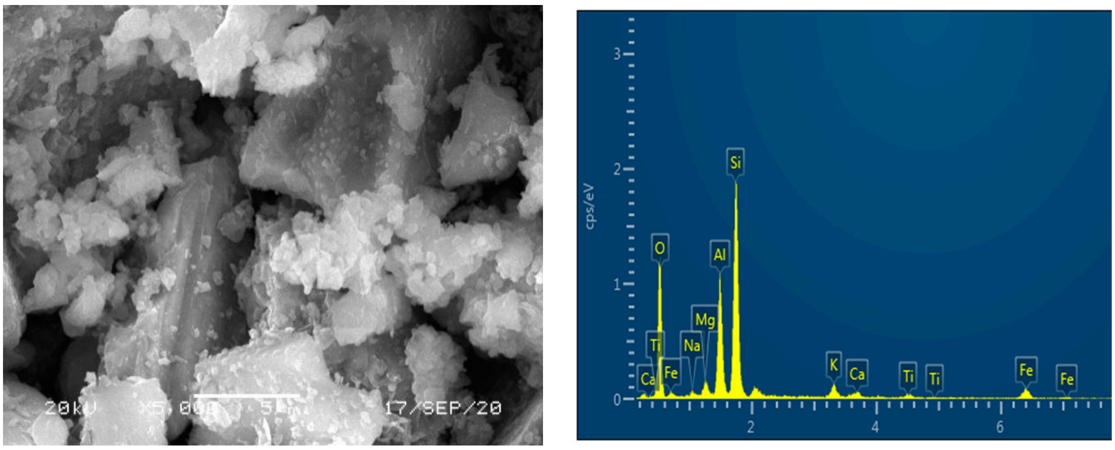

(**a**) (**b**)

Figure 3. (**a**) SEM, (**b**) EDS. Micro characteristics of Portland cement.

Table 3. Physical and mechanical indexes of cement.

Index	Fineness (%)	Initial Setting Time (min)	Final Setting Time (min)	Loss on Ignition (%)	28d Compressive Strength (MPa)	28d Flexural Strength (MPa)
Value	3.5	210	295	1.3	47.0	8.2

Table 4. Physical and mechanical indexes of nano silica.

Index	Loss on Ignition (%)	Bulk Density g/cm^3	Specific Area (m^2/kg)	pH Value
Value	1	3.06	200,000	3.4~4.7

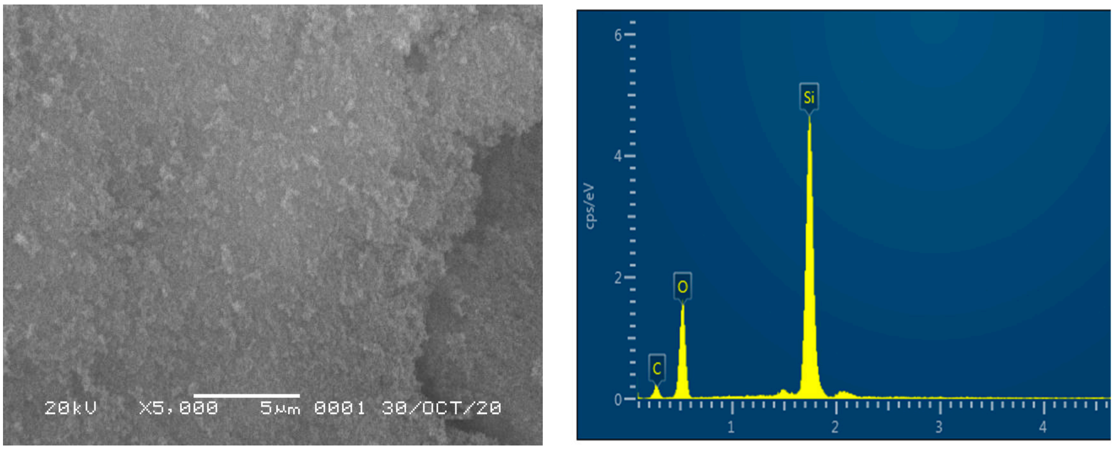

(**a**) (**b**)

Figure 4. (**a**) SEM, (**b**) EDS. Microscopic characteristics of nano silica.

2.2. Test Scheme

According to the application scenarios of cemented soil in actual projects, the moisture content of soil was set at 80%. The test was divided into two parts. First, the mechanical properties of TCS were studied, and the optimal iron tailing content was obtained. The cement content was set at 30% and the iron tailing content was set at 0, 10%, 20%, 30%, and 40%, respectively, to produce the TCS samples. Next, on the basis of the optimal iron tailing content, nano silica at contents of 0.5%, 1.5%, and 2.5% was added continuously to investigate the modification effect of nano silica on TCS. The content of cement, iron tailings and nano silica refers to the mass ratio in relation to dry soil. The test ages of all samples were 7d. The material composition and specific symbols of the samples are shown in Figure 5, and the specific test scheme is shown in Table 5.

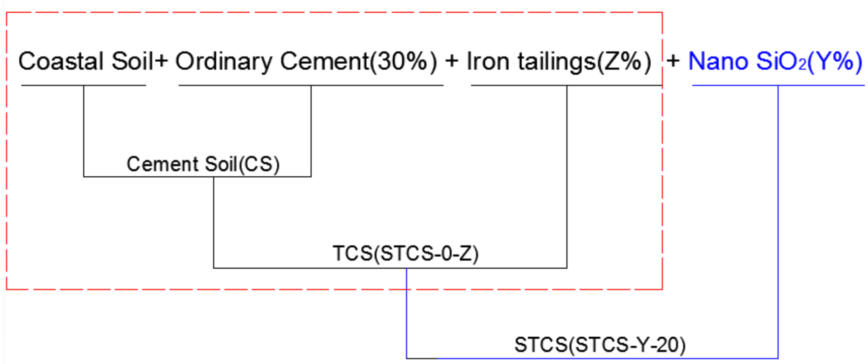

Figure 5. Material composition and specific symbols of the sample.

Table 5. Test scheme for STCS.

Sample Group	Cement Content/%	Iron Tailing Content/%	Nano Silica Content/%	Curing Age/d
STCS-0-0	30	0	0	7
STCS-0-10	30	10	0	7
STCS-0-20	30	20	0	7
STCS-0-30	30	30	0	7
STCS-0-40	30	40	0	7
STCS-0.5-X	30	Optimal content	0.5	7
STCS-1.5-X	30	Optimal content	1.5	7

Note: In STCS-Y-Z, Y represents the content of nano silica, Z represents the content of iron tailings, and the X represents the optimal content.

2.3. Sample Preparation and Maintenance

According to the requirements of the Chinese "GBT 50123-2019" standard, the main process of the sample preparation is shown in Figure 6.

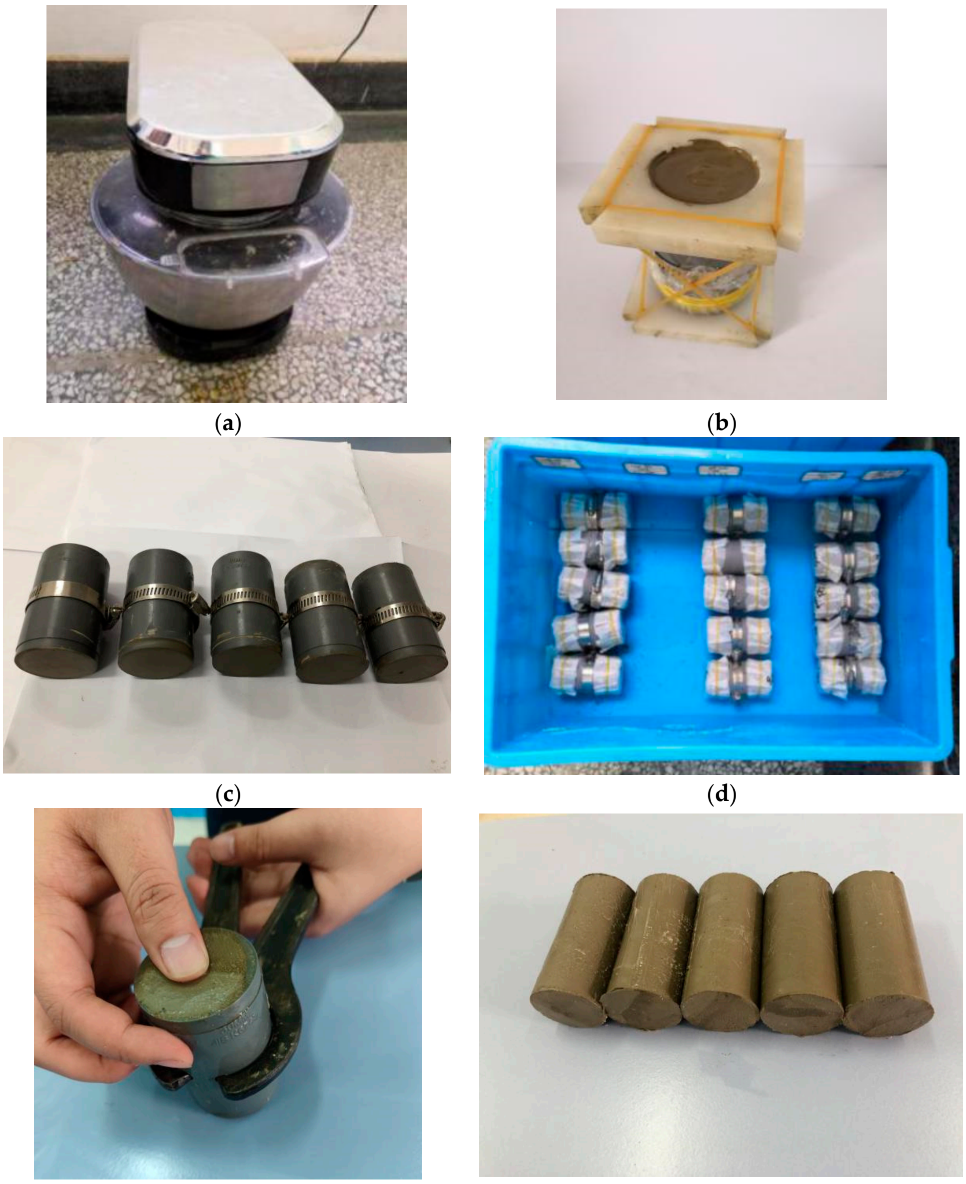

(**a**) (**b**) (**c**) (**d**) (**e**) (**f**)

Figure 6. (**a**–**f**) Main processes of sample preparation.

(1) An appropriate amount of wet soil was placed into the mixer, and mixed well; the cement slurry was prepared according to the test mix ratio, then poured into the mixer and mixed evenly, as shown in Figure 6a.

(2) Iron tailings and nano silica were added into the mixer in turn, and were stirred twice, for 4 minutes each time, to ensure that the test materials were fully and evenly mixed. The mixed materials that had been stirred were put into a grouting bag, and were then added to the standard mold three times to ensure the same height each time. The diameter of the mold was 39.1mm, and the height was 80mm. After each feeding, manual vibration was required for about 40 times until it was dense, as shown in Figure 6b.

(3) The sample was left to stand for about 2h. After it was initially set, both ends of the molds were removed and smoothed with a spatula, as shown in Figure 6c. The metal clip outside the test mold was mainly used to apply tightening force to the test mold to ensure the forming of the sample. When demolding the sample, the metal clip was first removed.

(4) Filter paper and rubber bands were used to bind both ends of the sample, and then put in water for curing, as shown in Figure 6d.

(5) After reaching 7d, the sample was removed from the mold using the special demolding tool, as shown in Figure 6e. Then, the sample was placed in a safe place and prepared for subsequent tests, as shown in Figure 6f.

3. Unconfined Compressive Test Analysis of TCS

3.1. Stress–Strain Curve Analysis

Five repeated tests were carried out for each group of samples, and five stress–strain curves were obtained. The stress–strain curves of TCS with different iron tailing contents are summarized in Figure 7, which are all softening curves.

3.2. Curve Normalization

Due to the contingency and error in the unconfined compressive test, based on the research results of Long Hongbo et al. [34], the deviation between the peak points of different stress–strain curves was taken as the research object, and an improved weighted average method was proposed to optimize the curves of five repeated tests by using the weight of each peak point. The detailed calculation steps are as follows:

(1) Determining the standard value. First, the peak point is mean processed to obtain a set of standard values, as shown in Formula (1). N represents the number of tests, in this test, $N = 5$; $i \in [1, N]$ is the peak stress of each curve; q^{-} is the mean stress.

$$q^{-} = \frac{1}{N}\sum_{i=1}^{N} q_i \tag{1}$$

(2) Determining the deviation. The peak stress of each peak point is subtracted from the standard stress, and its absolute value is deviation p_i, as shown in Formula (2).

$$p_i = \left|q_i - q^{-}\right| \tag{2}$$

(3) Determining the degree of deviation. The variance M is introduced to describe the degree of deviation between each peak stress and the standard stress, as shown in Formula (3).

$$M = \frac{1}{N}\sum_{i=1}^{N} \left(q_i - q^{-}\right)^2 \tag{3}$$

(4) Selecting the weighted weight. In order to determine the weight of each peak stress, each deviation value is divided by the variance M, respectively, to obtain the weighted weight W of each peak stress, as shown in Formula (4).

$$W = \frac{p_i}{M} \tag{4}$$

(5) Determining the weight function. The weighted weight W of each peak stress and standard stress can be obtained from Formula (4). However, this weight does not conform to the traditional weighting law, which needs to be transformed to a certain extent. Combined with the above analysis, the use of a weight function to transform the initial weight is proposed, as shown in Formula (5).

$$C(x) = \frac{1}{2}\cos^{N}(\pi x + 1) \tag{5}$$

where x is the independent variable and $C(x)$ is the dependent variable; N can be valued according to the actual situation, and its function is to improve the accuracy of the calculation results; in this test, $N = 5$.

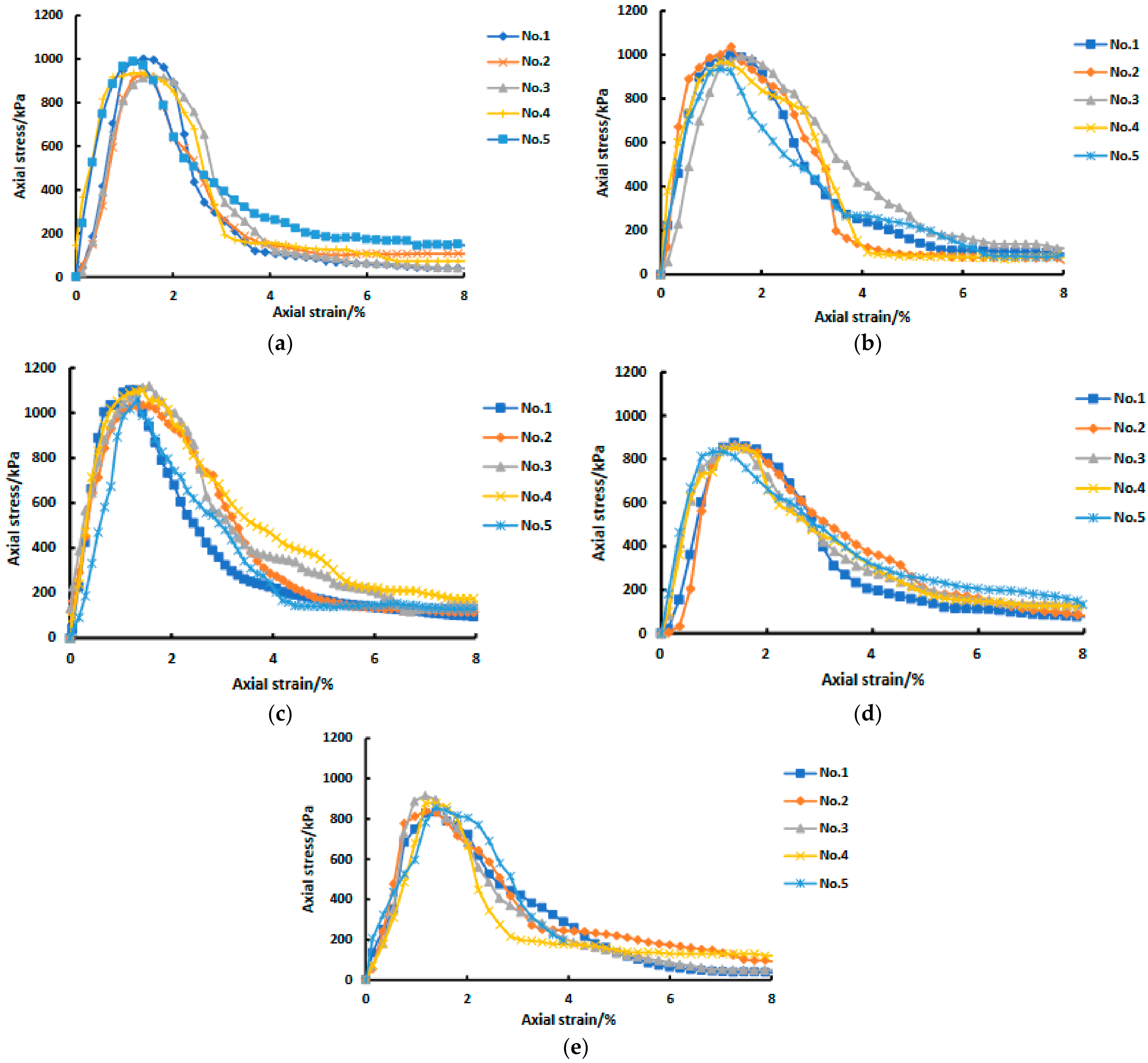

Figure 7. Stress–strain curves of TCS with different iron tailing contents. (**a**) STCS-0-0; (**b**) STCS-0-10; (**c**) STCS-0-20; (**d**) STCS-0-30; (**e**) STCS-0-40.

1. Determining the weight. In order to determine whether Formula (5) is feasible, Formula (4) is substituted into the weight function $G(x)$ to obtain the final weight R, as shown in Formula (6).

$$R = C(W) = \frac{1}{2}\cos^N(\pi W + 1) \tag{6}$$

2. Determining the weighting factor. In order to obtain the weighting factor of each peak stress, the weights obtained from Formula (6) are divided by the weight sums, as shown in Formula (7).

$$Y_i = \frac{R}{\sum\limits_{i=1}^{N} R} \tag{7}$$

3. Determining the weighted stress. Each weighting factor obtained in Formula (7) is multiplied by the corresponding peak stress, and the value of each peak stress in the weighted stress can be obtained. The final weighted peak stress q_m can be obtained by adding them together, as shown in Formula (8).

$$q_m = \sum_{i=1}^{N} q_i Y_i \tag{8}$$

It can be seen from above that there were five stress–strain curves for each group of samples, the peak points of the five curves of STCS-0-0 were taken as reference to perform a weighted average, and the obtained specific gravity was multiplied by the standard curve to obtain the q-ε representative curve of the test. In order to verify the applicability of this method, the calculation results were compared with the original curve, and the comparison results are shown in Figure 8. The results show that the representative q-ε curve obtained by the new method has a good correlation with the original q-ε curve.

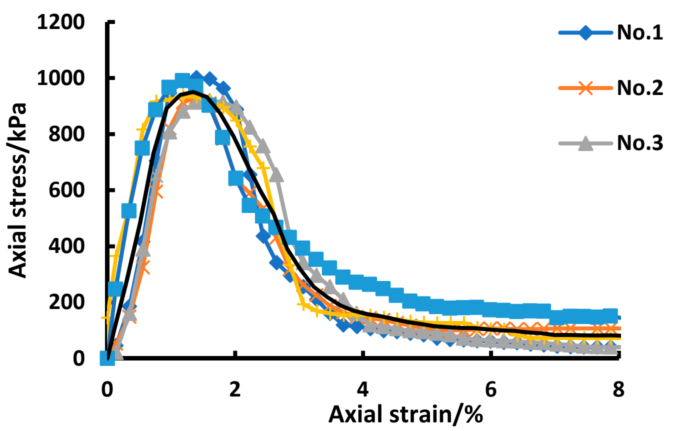

Figure 8. q-ε curve of STCS-0-0.

3.3. Peak Strength and Peak Strain Analysis

The peak strength is the maximum stress value on the stress–strain curve of the unconfined compressive test of the soil. The peak strain is the strain corresponding to the peak strength. According to the method in Section 3.2, the peak strength and peak strain of various types of cemented soil are summarized in Table 6. Table 6 shows that the peak strengths of STCS-0-0, STCS-0-10, and STCS-0-20 were 955kPa, 986kPa, and 1080kPa, respectively. When the iron tailing content was 10% and 20%, the peak strength of TCS was 3% and 13% higher than that of CS, respectively. When the iron tailing content continued to increase, the unconfined compressive strength of TCS began to decrease, and the iron tailings began to show a deterioration effect, which gradually increased with the increase in the iron tailing content. It can be found from Hou Rui's research that when the iron tailing content was less than 25%, iron tailings had a certain improvement effect on the compressive strength of CS, which was consistent with the results in this paper [35].

Table 6. Peak strength and peak strain of each group of TCS.

Sample No.	Peak Strength (kPa)	Average Error of Peak Strength (kPa)	Peak Strain (%)	Average Error of Peak Strain (%)
STCS-0-0	955	35	1.346	0.135
STCS-0-10	986	27	1.348	0.135
STCS-0-20	1080	29	1.379	0.082
STCS-0-30	857	12	1.347	0.132
STCS-0-40	863	26	1.303	0.102

The peak strain of TCS with different iron tailing contents fluctuated between 1.303 and 1.379. When the iron tailing content was 20%, the peak strain increased the most, but only by 2%. The addition of iron tailings had little effect on the peak strain of CS.

Iron tailings can be categorized as a high-silicon type ultra-fine tailing sand. Their particle size is larger than that of clay particles, and thus, they act as a coarse aggregate in soil. The addition of iron tailings in small quantities can improve the gradation of soil particles and reduce the internal pores of the soil. Under the action of cementitious substances formed by cement hydration and consolidation, iron tailings and soil particles clump together to form a whole structure, so as to improve the soil's compressive strength. With the increase in the iron tailing content, the proportion of iron tailings in the composite cemented soil increases, the properties of the composite material begin to approach the sand soil, the internal structure of the soil begins to loosen, the cohesion between particles decreases, and the compressive strength of the soil decreases.

3.4. Residual Strength Analysis

According to "GBT 50123-2019", the sample is defined as damaged when the strain reaches the peak strain in the unconfined compressive stage, and the stress measured at 5% strain, after the selection of the peak strain, is selected as the residual strength. The residual strength of TCS is summarized in Table 7.

Table 7. Residual strength of each group of TCS.

Sample No.	Residual Strength (kPa)	Average Error of Residual Strength (kPa)
STCS-0-0	82	33
STCS-0-10	93	20
STCS-0-20	132	27
STCS-0-30	110	14
STCS-0-40	89	42

It can be seen from Table 7 that iron tailings have a greater impact on the residual strength of TCS. When the iron tailing content is 20%, the residual strength of TCS reaches its peak, which is increased by 60% compared with that of CS. When the iron tailing content continues to increase, the residual strength of TCS begins to decrease, and its mechanism of action is similar to the peak strength.

3.5. Elastic Modulus Analysis

The elastic moduli of TCS are summarized in Figure 9.

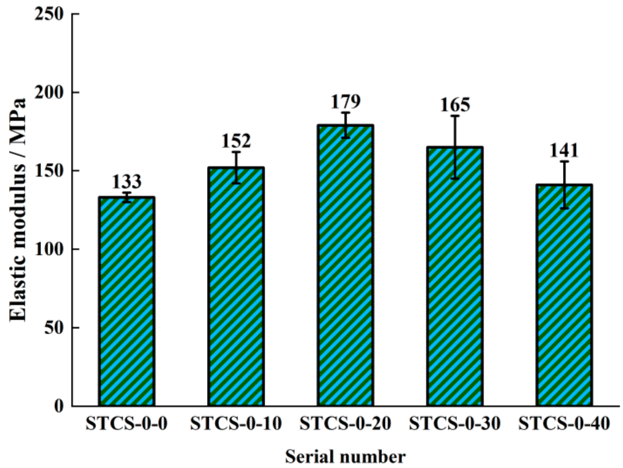

Figure 9. Elastic moduli of TCS.

It can be seen from Figure 9 that after adding 10%, 20%, 30%, and 40% iron tailings, the elastic modulus of TCS increased by 14%, 35%, 24%, and 6%, respectively. When the iron tailing content was 20%, the elastic modulus increased the most.

4. Unconfined Compressive Test Analysis of STCS

4.1. Stress–Strain Curve Analysis

Under the condition that the optimal iron tailing content was 20%, 0.5%, 1.5%, and 2.5% quantities nano silica content were added to modify TCS. The stress–strain curves of STCS with different nano silica contents are summarized in Figure 10, which are all softening curves.

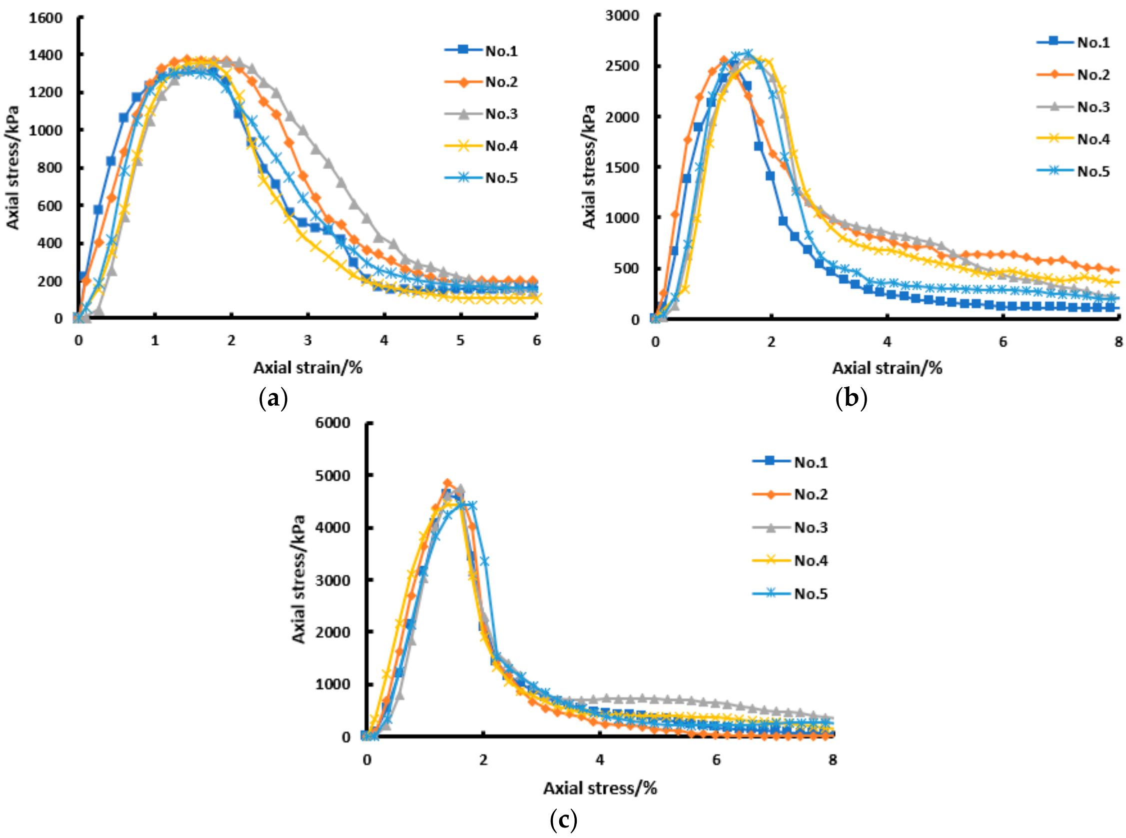

Figure 10. Stress–strain curve of STCS. (**a**) STCS-0.5-20; (**b**) STCS-1.5-20; (**c**) STCS-2.5-20.

4.2. Peak Strength and Peak Strain Analysis

The peak strength and peak strain of STCS are summarized in Figures 11 and 12.

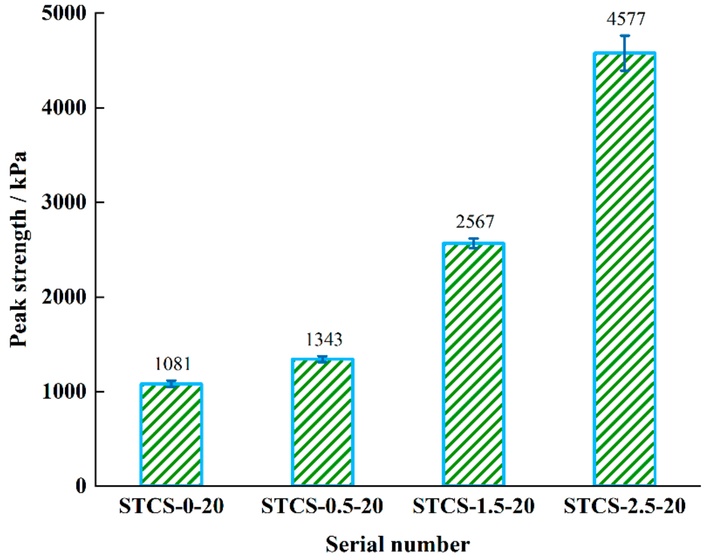

Figure 11. Peak strength of STCS.

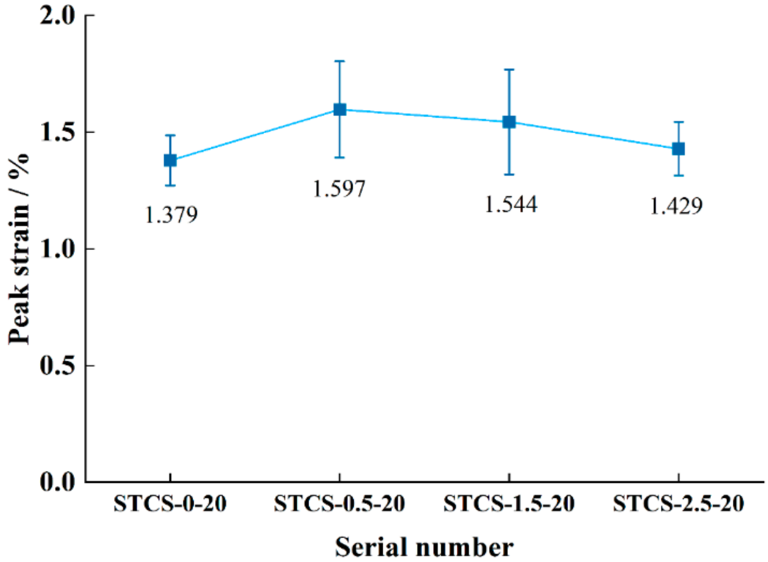

Figure 12. Peak strain of STCS.

It can be seen from Figure 11 that after adding 0.5%, 1.5%, and 2.5% nano silica, the compressive strength of TCS increased by 24%, 137%, and 323%, respectively, which significantly enhanced the compressive strength of TCS.

The peak strain represents the strain variable when the sample reaches the peak stress. The larger the peak strain is, the later the sample reaches failure, which is of great significance in engineering applications. It can be seen from Figure 12 that nano silica increased the peak strain of TCS, but with the increase in the nano silica content, the increment gradually decreased. When the nano silica content was 0.5%, the peak strain of TCS increased by 15%, which indicates that nano silica can help to delay the time of sample failure, but the effect is limited. Because with the increase in nano silica content, the brittleness of the material was also increasing, the increment of peak strain of TCS began to decrease.

4.3. Residual Strength Analysis

The residual strength of STCS is summarized in Table 8.

Table 8. Residual strength of each group of STCS.

Sample No.	Residual Strength (kPa)	Average Error of Residual Strength (kPa)
STCS-0-20	132	27
STCS-0.5-20	152	23
STCS-1.5-20	277	128
STCS-2.5-20	174	144

Table 8 shows that the addition of nano silica effectively improves the residual strength of TCS. When the nano silica content was 0.5%, the residual strength increased by 20kPa; when the nano silica content was 1.5%, the residual strength increased by 142kPa; but when the nano silica content reached 2.5%, the residual strength increased by only 42kPa. The increment of the residual strength of TCS by adding nano silica shows a trend of first increasing and then decreasing, and of reaching the maximum when the nano silica content is 1.5%, which is consistent with the increasing of the peak strength of STCS.

4.4. Elastic Modulus Analysis

The elastic modulus of STCS are summarized in Figure 13.

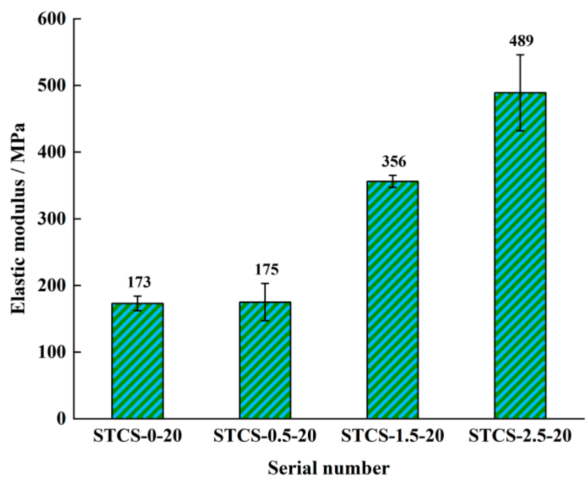

Figure 13. Elastic modulus of STCS.

It can be seen from Figure 13 that after adding 0.5%, 1.5%, and 2.5% nano silica, the elastic modulus of STCS increased by 1%, 106% and 183%, respectively. which significantly enhanced the elastic modulus of TCS.

5. Microscopic Mechanism Analysis

5.1. SEM Test Analysis

In order to better analyze the strength growth mechanism of STCS, the microscopic morphology of various cement soils was observed by SEM. Four groups of unconfined samples of STCS-0-0, STCS-0-20, STCS-0-40, and STCS-2.5-20 were selected for microscopic testing. Via SEM scanning with an electron microscope, four groups of microstructure photos of STCS were obtained at 5000 times magnification, as shown in Figure 14.

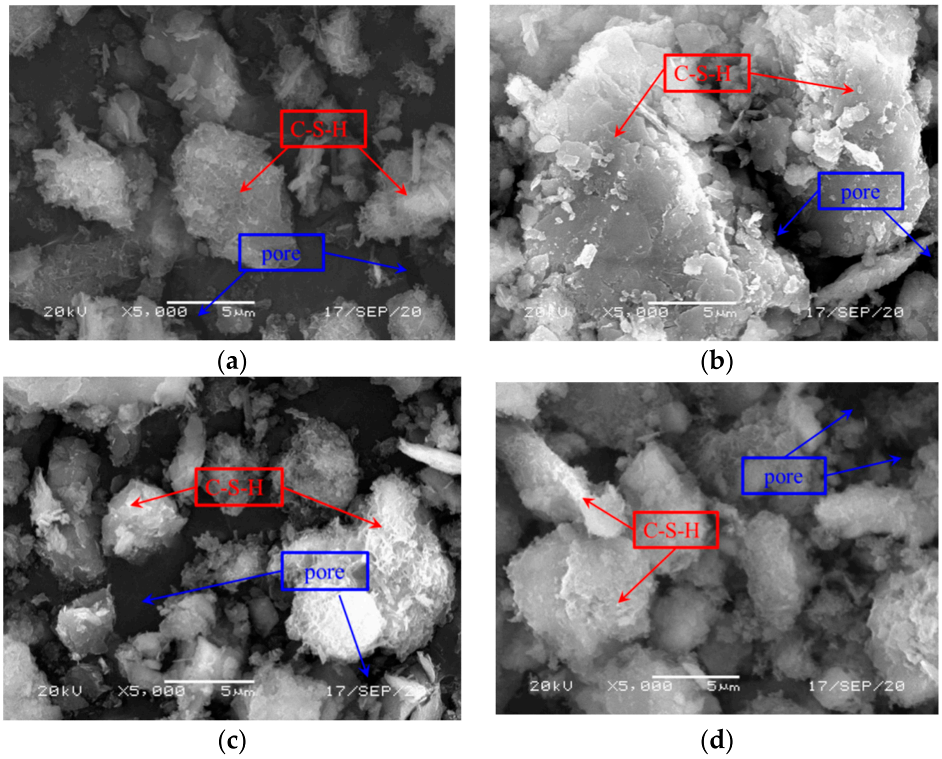

Figure 14. SEM images of different types of STCS. (**a**) STCS-0-0; (**b**) STCS-0-20; (**c**) STCS-0-40; (**d**) STCS-2.5-20.

Figure 14 shows that a large amount of hydration products were produced in each group of samples, including a relatively large amount of flocculated colloid C-S-H, which has strong adsorption capacity. The internal particles of CS are of different sizes and there are many pores. When 20% iron tailings was added, it can be seen from the microscopic image that there were particles of different sizes in the composite cemented soil, forming a good gradation. Some iron tailings particles filled the large particles in the soil, and a large amount of flocculated colloid C-S-H was adsorbed on the soil particles, forming a stable whole structure with iron tailings. The composite cemented soil mixed with 40% iron tailing content was mostly composed of medium and small units, and the gaps between the particles were large and not well filled.

The characteristics of nanomaterials effectively played their role in the improvement of TCS with 2.5% nano silica content. It can be seen from the microscopic pictures of STCS-2.5-20 that the structure was very compact, and the nano silica adequately filled the pores of the composite cemented soil.

5.2. SEM Image Processing

The basic properties of CS depend largely on its particle bonding characteristics at the microscopic level, and the macro-mechanical performance of CS largely depends on the pore size at the microscopic level. In order to quantitatively evaluate the relationship between the compressive strength of CS and the size of microscopic pores, the SEM image obtained at 5000 times magnification was binarized to obtain the quantitative pore size of relevant samples, as shown in Table 9.

Table 9. Porosities of different STCS.

Sample No.	STCS-0-0	STCS-0-20	STCS-0-40	STCS-2.5-20
Porosity	0.334	0.225	0.448	0.098

Table 9 shows that the porosity of the four types of STCS samples, from high to low, was STCS-0-40 > STCS-0-0 > STCS-0-20 > STCS-2.5-20. This is consistent with the order of the unconfined compressive strength of each group of STCS samples.

Compared with STCS-0-0, the porosity of STCS-0-20 was reduced by 32%, which shows that the compressive strength of STCS with 20% iron tailing content was improved compared with that of CS. The porosity of STCS-0-40 was higher than that of STCS-0-0, which was because the particle size of iron tailings was larger than that of clay particles; the proportion of fine particles in the mixture decreased due to the increasing of the iron tailing content, which was not enough to fill the pores between the cement and the soil. As a result, the fine aggregate particle gradation became worse after the iron tailing content exceeded 20%. Compared with STCS-0-20, the porosity of STCS-2.5-20 was reduced by 56%. It can be seen that the internal pores of STCS were very small and the structure was compact. Therefore, the unconfined compressive strength of STCS with 2.5% nano silica content reached more than three times that of TCS.

6. Conclusions

The mechanical properties and micro mechanism of TCS and STCs at 7d curing age were studied by unconfined compressive strength test and SEM test. The following conclusions can be drawn.

(1) With the increase in the content of iron tailings, the unconfined compressive strength, peak strain, residual strength, and elastic modulus of TCS first increased and then decreased. The optimal content of iron tailings was 20%.

(2) Nano silica could significantly modify the unconfined compressive strength and elastic modulus of TCS. The unconfined compressive strength of STCS increased with the increasing of the nano silica content. Compared with STCS-0-20, the unconfined compressive strength of STCS-0.5-20, STCS-1.5-20, and STCS-2.5-20 was increased by 24%, 137%, and 323% respectively. At the same time, the addition of nano silica effectively improved the peak strain and residual strength of the TCS. With the increasing of the nano silica content, the peak strain, residual strength and elastic modulus first increased and then decreased.

(3) Analysis of SEM pictures showed that the flocculation colloid C-S-H generated by cement hydration and the porosity of the samples were the main factors affecting the strength of TCS and STCS. An appropriate amount of iron tailings can fill the pores in TCS. With the increase of iron tailings, the porosity of TCS increased, resulting in the decreasing of the strength. In addition, on the one hand, nano silica can promote the hydration reaction of cement and improve the cementation of particles in STCS. On the other hand, nano silica can fill the pores between particles and improve the compactness of STCS.

The above conclusions are based on the test data of 7d curing age. The strength of TCS and STCs will gradually increase with the curing age, and final strength of the composite may be achieved after 2–3 months.

Author Contributions: Conceptualization, X.S. and H.X.; investigation, D.Z. and K.Y.; formal analysis, F.T. and P.J.; writing—review and editing, W.W. All authors have read and agreed to the published version of the manuscript.

Funding: This research was funded by the National Natural Science Foundation of China, grant number 41772311, and the Shandong Provincial Natural Science Foundation, grant number ZR202102240826.

Data Availability Statement: The data presented in this study are available on request from the corresponding author.

Acknowledgments: This authors thank Linxia Wang from the Micro Testing Center of Shaoxing University for her help in the process of micro testing.

Conflicts of Interest: The authors declare no conflict of interest.

References

1. Aline, C.; Gustavo, C.X.; Jonas, A.; Leonardo, G.P.; Afonso, R.G.A.; Carlos, M.F.V.; Sergio, N.M. Environmental durability of soil-cement block incorporated with ornamental stone waste. In *Materials Science Forum*; Trans Tech Publications Ltd.: Kapellweg, Switzerland, 2014; Volume 798, pp. 548–553.
2. Datta, S.G.; Roy, D. Influence of flow velocity and nutrient availability on microbially mediated reduction of erosion suscep-tibility of sand. In *Geotechnics for Sustainable Infrastructure Development*; Springer: Singapore, 2020; pp. 945–950.
3. Liu, Y.; Lee, F.H.; Quek, S.T.; Chen, E.J.; Yi, J.T. Effect of spatial variation of strength and modulus on the lateral compression response of cement-admixed clay slab. *Géotechnique* **2015**, *65*, 851–865. [CrossRef]
4. Li, N.; Zhu, Y.; Zhang, F.; Lim, S.M.; Wu, W.; Wang, W. Unconfined compressive properties of fiber-stabilized coastal cement clay subjected to Freeze–Thaw cycles. *J. Mar. Sci. Eng.* **2021**, *9*, 143. [CrossRef]
5. Liu, Y.; He, L.Q.; Jiang, Y.J.; Sun, M.M.; Chen, E.J.; Lee, F.-H. Effect of in situ water content variation on the spatial variation of strength of deep cement-mixed clay. *Géotechnique* **2019**, *69*, 391–405. [CrossRef]
6. Rybak, J.; Adigamov, A.; Kongar-Syuryun, C.; Khayrutdinov, M.; Tyulyaeva, Y. Renewable-Resource technologies in mining and metallurgical enterprises providing environmental safety. *Minerals* **2021**, *11*, 1145. [CrossRef]
7. Rybak, J.; Gorbatyuk, S.M.; Bujanovna-Syuryun, K.C.; Khairutdinov, A.M.; Tyulyaeva, Y.S.; Makarov, P.S. Utilization of mineral waste: A method for expanding the mineral resource base of a mining and smelting company. *Metallurgist* **2021**, *64*, 851–861. [CrossRef]
8. Muguda, S.; Lucas, G.; Hughes, P.N.; Augarde, C.E.; Perlot, C.; Bruno, A.W.; Gallipoli, D. Durability and hygroscopic behaviour of biopolymer stabilised earthen construction materials. *Constr. Build. Mater.* **2020**, *259*, 119725. [CrossRef]
9. Bastos, L.A.D.C.; Silva, G.C.; Mendes, J.C.; Peixoto, R.A.F. Using iron ore tailings from tailing dams as road material. *J. Mater. Civ. Eng.* **2016**, *28*, 04016102. [CrossRef]
10. Hou, R.; Chen, S.l.; Ma, X.; Hu, Y.T. Study on mechanical properties of iron tailings sand-cement composite soil. *Sino-Foreign Highw.* **2019**, *39*, 206–209.
11. Tang, K.; Mao, X.S.; Xu, W.; Tang, X.L. Performance analysis of cement concrete mixed with fine aggregate of iron tailings. *Ind. Archit.* **2019**, *8*, 153–157.
12. Bao, W.B.; Di, G.H.; Chen, S.l.; Li, W.F. Study on toughening properties of high performance environmental friendly tailings sand cement-based composites. *Funct. Mater.* **2016**, *47*, 7–12. [CrossRef]
13. Simonsen, A.M.T.; Solismaa, S.; Hansen, H.K.; Jensen, P.E. Evaluation of mine tailings' potential as supplementary cementi-tious materials based on chemical, mineralogical and physical characteristics. *Waste Manag.* **2020**, *102*, 710–721. [CrossRef]
14. Long, G.; Li, L.; Li, W.; Ma, K.; Zhou, K.L. Enhanced mechanical properties and durability of coal gangue reinforced cement-soil mixture for foundation treatments. *J. Clean. Prod.* **2019**, *231*, 468–482. [CrossRef]
15. Consoli, N.C.; Godoy, V.B.; Tomasi, L.E.; Paula, T.M.D.; Bortolotto, M.S.; Favretto, E. Fibre-reinforced sand-coal fly ashlime-NaCl blends under severe environmental conditions. *Geosynth. Int.* **2019**, *26*, 525–538. [CrossRef]
16. Feng, R.; Wu, L.; Liu, D.; Wang, Y.; Peng, B. Lime- and Cement-Treated sandy lean clay for highway subgrade in China. *J. Mater. Civ. Eng.* **2020**, *32*, 04019335. [CrossRef]
17. Tebogo, M.; Thandiwe, S. Evaluation of chemically treated and lime stabilized gold mine tailings: Effect on unconfined compressive strength. *Key Eng. Mater.* **2019**, *803*, 366–370. [CrossRef]
18. Kumar, R.; Das, P.; Beulah, M.; Arjun, H.R. Geopolymer Bricks using iron ore tailings, slag sand, ground granular blast furnace slag and fly ash. In *Geopolymers and Other Geosynthetics*; IntechOpen: London, UK, 2020.
19. Falayi, T. A comparison between fly ash and basic oxygen furnace slag-modified gold mine tailings geopolymers. *Int. J. Energy Environ. Eng.* **2019**, *11*, 207–217. [CrossRef]
20. Festugato, L.; Consoli, N.; Fourie, A. Cyclic shear behaviour of fibre-reinforced mine tailings. *Geosynth. Int.* **2015**, *22*, 196–206. [CrossRef]
21. Chen, X.; Shi, X.; Zhou, J.; Chen, Q.; Li, E.; Du, X. Compressive behavior and microstructural properties of tailings polypropylene fibre-reinforced cemented paste backfill. *Constr. Build. Mater.* **2018**, *190*, 211–221. [CrossRef]
22. Cristelo, N.; Cunha, V.M.; Gomes, A.T.; Araújo, N.; Miranda, T.; Lopes, M.D.L. Influence of fibre reinforcement on the post-cracking behaviour of a cement-stabilised sandy-clay subjected to indirect tensile stress. *Constr. Build. Mater.* **2017**, *138*, 163–173. [CrossRef]
23. Lirer, S.; Flora, A.; Consoli, N.C. On the strength of Fibre-Reinforced soils. *Soils Found.* **2011**, *51*, 601–609. [CrossRef]
24. Ghasabkolaei, N.; Janalizadeh, C.A.; Roshan, N.; Ghasemi, S.E. Geotechnical properties of the soils modified with nanomaterials: A comprehensive review. *Arch. Civ. Mech. Eng.* **2017**, *17*, 639–650. [CrossRef]
25. Wang, W.; Zhang, C.; Li, N.; Tao, F.; Yao, K. Characterisation of nano magnesia–cement-reinforced seashore soft soil by direct-shear test. *Mar. Georesour. Geotechnol.* **2019**, *25*, 1–10. [CrossRef]
26. Yao, K.; An, D.L.; Wang, W.; Li, N.; Zhou, A. Effect of nano-MgO on mechanical performance of cement stabilized silty clay. *Mar. Georesour. Geotechnol.* **2020**, *38*, 250–255. [CrossRef]
27. Zheng, J.; Sun, X.; Guo, L.; Zhang, S.; Chen, J. Strength and hydration products of cemented paste backfill from sulphide-rich tailings using reactive MgO-activated slag as a binder. *Constr. Build. Mater.* **2019**, *203*, 111–119. [CrossRef]
28. Liu, H.; Xue, J.; Li, B.; Wang, J.; Lv, X.; Zhang, J. Effect of graphite tailings as substitute sand on mechanical properties of concrete. *Eur. J. Environ. Civ. Eng.* **2020**, *10*, 1–19. [CrossRef]

29. Sarkkinen, M.; Kujala, K.; Gehör, S. Efficiency of MgO activated GGBFS and OPC in the stabilization of highly sulfidic mine tailings. *J. Sustain. Min.* **2019**, *18*, 115–126. [CrossRef]
30. Li, N.; Lv, S.; Wang, W.; Guo, J.; Jiang, P.; Liu, Y. Experimental investigations on the mechanical behavior of iron tailings powder with compound admixture of cement and nano-clay. *Constr. Build. Mater.* **2020**, *254*, 119259. [CrossRef]
31. Wang, W.; Li, J.; Hu, J. Unconfined Mechanical Properties of Nanoclay Cement Compound Modified Calcareous Sand of the South China Sea. *Adv. Civ. Eng.* **2020**, *2020*, 6623710. [CrossRef]
32. Wang, W.; Li, Y.; Yao, K.; Li, N.; Zhou, A.Z.; Zhang, C. Strength properties of nano-MgO and cement stabilized coastal silty clay subjected to sulfuric acid attack. *Mar. Georesour. Geotechnol.* **2020**, *38*, 1177–1186. [CrossRef]
33. Liu, C.; Li, K.; Geng, Y.; Li, Q. Microstructure characteristics of soils with different land use types in the Yellow River Delta. *Trans. Chin. Soc. Agric. Eng.* **2020**, *36*, 81–87, (In Chinese with English abstract).
34. Long, H.; Ye, X.H.; Tan, S.W. Application of normalized weighted average algorithm in measurement. *Electr. Light Control.* **2010**, *17*, 68–70.
35. Chen, S.l.; Hou, R.; Ni, C.L.; Wang, J.X. Study on mechanical properties of cement soil based on triaxial compression test. *Silic. Bull.* **2018**, *37*, 4012–4017.